Nearly Massless Electrons in the Silicon Interface with a Metal Film

Keun Su Kim,[1] Sung Chul Jung,[2] Myung Ho Kang,[2] and Han Woong Yeom[1,2,*]

[1]*Center for Atomic Wires and Layers, Pohang University of Science and Technology, Pohang 790-784, Korea*
[2]*Department of Physics, Pohang University of Science and Technology, Pohang 790-784, Korea*

(Received 17 February 2010; published 16 June 2010)

We demonstrate the realization of nearly massless electrons in the most widely used device material, silicon, at the interface with a metal film. Using angle-resolved photoemission, we found that the surface band of a monolayer lead film drives a hole band of the Si inversion layer formed at the interface with the film to have a nearly linear dispersion with an effective mass about 20 times lighter than bulk Si and comparable to graphene. The reduction of mass can be accounted for by a repulsive interaction between neighboring bands of the metal film and Si substrate. Our result suggests a promising way to take advantage of massless carriers in silicon-based thin-film devices, which can also be applied to various other semiconductor devices.

DOI: 10.1103/PhysRevLett.104.246803 PACS numbers: 73.20.−r, 71.18.+y, 79.60.−i

The ultimate performance of electronic devices is largely governed by the effective mass of charge carriers. Therefore, the never-ending quest for higher performance devices has looked towards high speed carriers with a light effective mass [1]. This quest may have reached its ultimate goal through the recent findings of massless electrons with their speed close to light in graphene [2,3] and bismuth compounds [4–7]. However, for these materials various difficulties exist in promptly realizing practical and mass-producible devices.

In general, the effective mass of electrons is determined by their energy dispersion. In particular, the edge structures of conduction and valence bands near the energy gap (E_g) are important. In the band-edge region, the dispersion is sensitive to the interaction between the bottom conduction and the top valence band as described well by the $k \cdot p$ theory [8]. This standard theory provides an approximate analytic expression for band dispersion under the interband interaction around high-symmetry points of momentum (k) space [8]. The interaction energy, $\pm\sqrt{(E_g/2)^2 + (P \cdot k)^2}$ (where P is the optical matrix element), gives rise to repulsion between bands and provides the linear component in dispersion [8]. As E_g approaches zero, the dispersion becomes nearly linear $E(k) \approx P \cdot k$ with a much lighter effective mass of electrons $m^* = \hbar^2 E_g/(2P^2)$. This effect explains the trend that a semiconductor with a narrower gap has a lighter effective mass [9] and the zero-gap semiconductor of graphene has a negligible effective mass [2,3]. This theory also tells us that if the energy gap could be controlled, the effective mass would be tuned through the interband interaction. While the energy gap of bulk materials cannot be tuned easily as fixed by their crystalline structure, here we show that a similar effect can be obtained at a semiconductor interface where a proper interface state is formed within the band gap [10–12].

We chose an ultrathin (only single layer) Pb film on an n-type Si(111) substrate, which has ideally abrupt interfacial structure and strongly dispersing metallic electron bands within the Si band gap [13–15]. For this system, the film-substrate interaction, which is exploited in this work, was already invoked to explain the anomalous superconductivity at the two-dimensional (2D) limit [16,17]. Figure 1(a) illustrates the atomic structure of the interface with the Pb density of 1.2 monolayer (ML) (7.84 atoms/nm^2). Pb atoms are densely packed within a

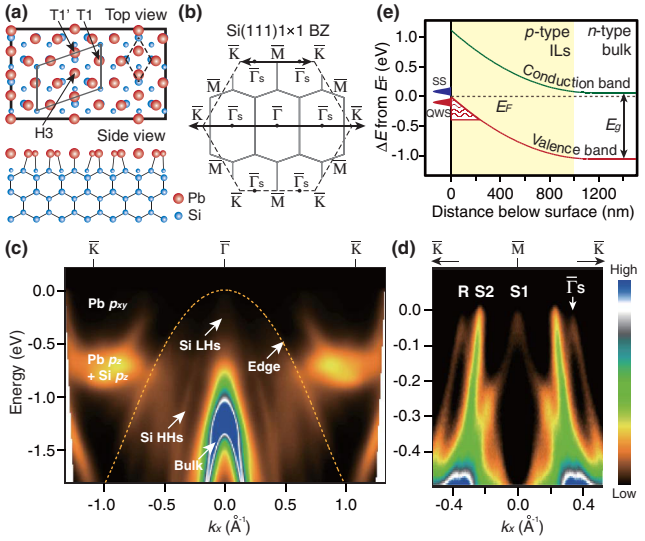

FIG. 1 (color online). (a) Crystal- and (b) reciprocal-lattice structures for Pb/Si(111) at 1.2 ML with a $\sqrt{7} \times \sqrt{3}$ symmetry [13]. Gray (dashed) line represents the $\sqrt{7} \times \sqrt{3}$ (1 × 1) surface unit cell. ARPES data collected along (c) long and (d) short arrows in (b) crossing 1 × 1 ($\bar{\Gamma}$) and $\sqrt{7} \times \sqrt{3}$ ($\bar{\Gamma}_S$) Brillouin zone centers, respectively. The dashed line in (c) denotes the Si valence-band edge. Λ-shaped band with a linear dispersion on each $\bar{\Gamma}_S$ in (d) is labeled R and two other gap-state bands in between are denoted by $S1$ and $S2$. Both ARPES images are symmetrized with respect to the origin. (e) Band bending in the present n-type Si substrate calculated by the measured E_F position and the bulk doping concentration [20].

single layer upon the bulk-terminated Si(111) surface [13]. Most of the Pb atoms sit on top of underlying Si atoms ($T1$ or $T1'$ sites) while part of them are slightly displaced ($T1'$) by additional Pb atoms in hollow sites (H3), which lead to the formation of a uniform $\sqrt{7} \times \sqrt{3}$ unit cell [gray lines in Fig. 1(a)] [18]. Because of the anisotropy of this unit cell and the threefold symmetry of the substrate, one inevitably obtains triply rotated domains [15,18], which should be considered in interpreting experimental data.

Angle-resolved photoemission (ARPES) measurements were conducted in an ultrahigh vacuum chamber (6.5×10^{11} torr) equipped with a hemispherical electron analyzer (R4000, VG Scienta) and a high-flux He discharge lamp for 21.2 eV photons. The samples were cryogenically cooled down to 90–100 K for measurements. The overall energy and momentum resolutions were better than 20 meV and 0.02 Å^{-1}. Figure 1(c) shows band dispersions along the high-symmetry direction through the center of Brillouin zone $\bar{\Gamma}$ [the long arrow in Fig. 1(b)] measured by ARPES. Near $\bar{\Gamma}$, an intense parabolic band is readily found, which is the well-known direct transition from bulk Si valence bands [19]. Another feature with strong intensity appears near each zone boundary ($\bar{K}$) with little dispersion around 0.7 eV, which is the covalent-type bonding state between Pb and Si [14]. In contrast, around $\bar{K}$, there are parabolic bands dispersing toward the Fermi energy (E_F), which were identified as due to 2D metallic electrons localized within the Pb layer (called $S2$ hereafter) [15]. This metallic surface state induces a huge upward band bending in the n-type substrate and forms a p-type inversion layer (IL) as shown in Fig. 1(e) [20]. The strong band bending yields a triangular potential well to confine electrons in the interface IL into 2D quantum well states (QWS) [10,20]. An IL state at interfacial layers is typically not easily probed by very surface sensitive ARPES, but, for an ultrathin metal film such as single-layer In on Si(111), a previous ARPES study traced its detailed dispersion [21]. We also found such IL states; two holelike bands are observed with weak intensity between the bulk and surface bands in Fig. 1(c). A relatively prominent band is identified as the so-called heavy-hole (HH) bands [21], but the other branch with a lighter effective mass, light-hole (LH) band, is barely observable as a weak and broad feature on top of the Si bulk band.

Although the LH band is not clear enough here [Fig. 1(c)] due to its weak intensity, we can map its dispersion clearly at the center of the surface Brillouin zone ($\bar{\Gamma}_S$) away from $\bar{\Gamma}$ as translated by the surface periodicity [12,21]. Figure 1(d) shows band dispersions taken through two such $\bar{\Gamma}_S$'s and the $\bar{M}$ point [the short arrow in Fig. 1(b)]. There are strongly dispersing bands with dominant intensity, crossing E_F at ± 0.21 Å^{-1}, which correspond to the $S2$ state for Pb metallic electrons. In addition, two other bands are identified: $S1$ folded back near E_F with respect to $\bar{M}$ and R folded with respect to $\bar{\Gamma}_S$. Surprisingly, their dispersions are Λ shaped and apparently very linear, especially for R. The detailed dispersion of R, located on $\bar{\Gamma}_S$ and related to the Si LH band below, can be shown more clearly and quantified by the peak positions of momentum distribution curves (MDCs) in Fig. 2(c). The dispersion is indeed linear within the experimental uncertainty as shown in Fig. 2(b) (open circles). Thus, the effective mass value would be extremely small and cannot be quantified by a simple parabolic fit of the dispersion as in the case of graphene [3] and Bi compounds [5–7]. Instead, the Fermi velocity can straightforwardly be extracted from the slope of the band and is as high as $4.6 \pm 0.4 \times 10^5$ m/s, which reaches to half of those in graphene [3,18] and $Bi_{0.9}Sb_{0.1}$ [5], and is similar to those in Bi_2Se_3 [6] and Bi_2Te_3 [7]. The effective mass value of this linear band will be discussed further below.

Since the R band with a striking dispersion cannot be found in Si bulk crystals [Fig. 2(b)] and on clean Si(111) surfaces [19], it must be due to electron states localized at the interface (Si ILs) or within the Pb layer. To identify the origin of each band further, we performed theoretical calculations based on density functional theory (DFT). The calculations were performed using the Vienna *ab initio* simulation package within the generalized gradient approximation and the ultrasoft pseudopotential scheme with a plane wave basis [22]. The surface is modeled by a periodic slab geometry with 6 and 12 Si layers whose bottoms are terminated by hydrogen.

Figure 3(a) shows the calculated constant energy contours at E_F. There are two kinds of surface-state Fermi contours, pointlike crossings and wavy lines repeated following the surface periodicity. Since ARPES detects signals coming from all triply rotated domains, the expected Fermi contours result in a complex pattern [Fig. 3(b)]. Nevertheless, the agreement between the calculated and experimental Fermi contours is excellent in Figs. 3(c) and 3(d). The pointlike crossings and the details of the wavy con-

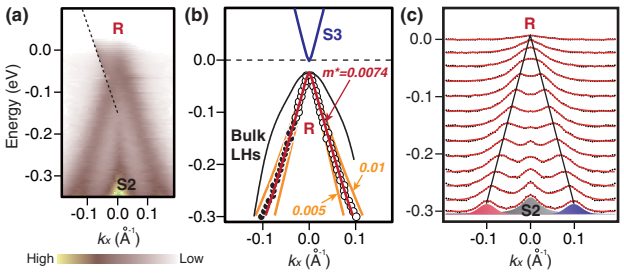

FIG. 2 (color online). (a) ARPES data of the R band. Data below the dashed line are those symmetrized with respect to $\bar{\Gamma}_S$ to eliminate the strong neighboring feature $S2$. (b) Spectral peak positions of the R band (open circles) extracted from MDCs shown in (c). Data points given in closed circles are those symmetrized. The dispersion of a normal Si LH band (black parabola) is compared to show the reduction of curvature. R and $S3$ lines are the results of $k \cdot p$ model fit [25]. The error bar in k is less than ± 0.02 Å^{-1}, which brackets the quantified effective mass (orange lines) (see also the supplementary material [18]). Red lines overlaid in (c) show fits by Lorenzian functions.

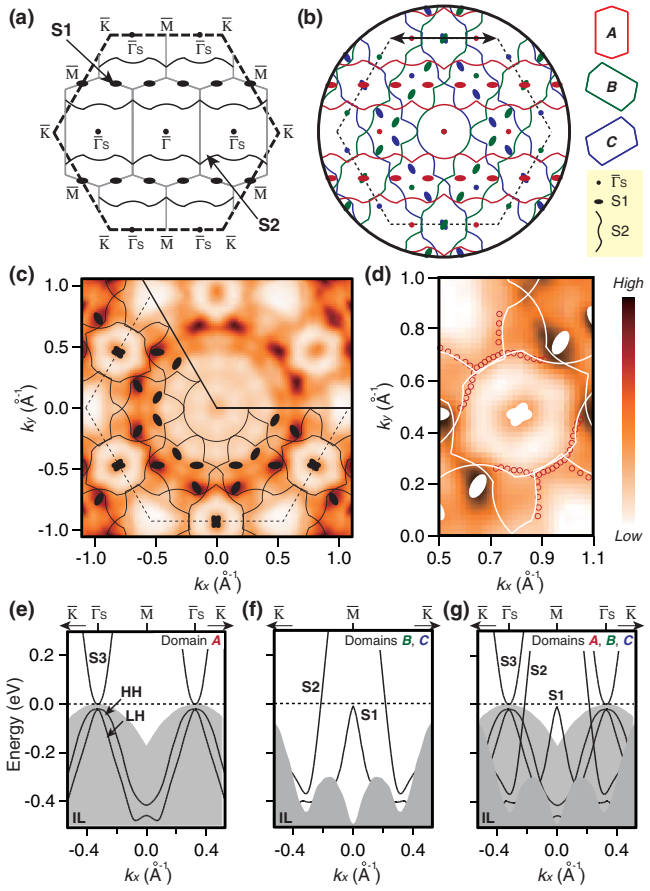

FIG. 3 (color online). Constant energy contours at E_F calculated from DFT for the (a) single-domain and (b) triply domain surfaces. Contours from each domain (A, B, and C) are indicated by different colors in (b). (c) ARPES constant energy contours at E_F. The DFT contours from (b) are superimposed. The raw data (region without DFT contours) are symmetrized reflecting the fundamental mirror symmetry. (d) Enlarged data around $\bar{M}$ for the detailed comparison between theory (white lines) and experiment (red circles extracted by MDC peak positions). DFT band dispersions along the arrow in (b) for (e) domain A and (f) domains B and C, which are overlapped together in (g). The shaded area represents the projected bulk band. For the best match with the experimental data the calculated surface-state energies are rigidly shifted by 120 meV with respect to Si bands.

tours are all precisely reproduced, which correspond to $S1$ and $S2$, respectively. The dispersions of $S1$ and $S2$ are also reproduced quantitatively well in the calculation [Fig. 3(f)]. These states come from the Pb layer due to in-plane Pb $5p$ orbitals. In fact, $S1$ and $S2$ bands are doubly degenerated with contributions from domains B and C overlapped exactly [Figs. 3(f) and 3(b)]. The contribution from domain A, which pass through two $\bar{\Gamma}_S$ points [Figs. 3(e) and 3(b)], is not degenerated. For this domain, the Pb-derived band ($S3$) is located just above E_F and two Si-derived bands below E_F at $\bar{\Gamma}_S$ [Fig. 3(e)]. The calculated electron density for the latter is distributed within Si layers, and their dispersions are consistent with the Si IL states (LH and HH) mentioned above. In particular, one with a sharper dispersion (LH) is very similar to R as compared in Fig. 2(b). The calculation, thus, clearly identifies $S1$, $S2$, $S3$, and R bands as three $5p$ states of the Pb layer and a Si-derived state, and reproduces the dispersions of $S1$, $S2$, and $S3$ quantitatively well. This result is consistent with the very recent work in Ref. [23] for the single-domain surface.

One notable feature of the calculation is that the bottom of the $S3$ band lies on E_F, namely, just above the experimentally measured band R with a very small energy separation. Thus, $S3$ has a chance to interact strongly with R from Si subsurface layers through the interband interaction [8]. As mentioned above, this interband interaction determines the effective mass of the bands according to the $k \cdot p$ model [8]. Indeed, such an interaction between the band of a Ag monolayer film and the band of a Si(111) substrate was observed recently and affects the dispersion of a $S3$-like surface state of Ag [24].

The fitting of our experimental dispersion using the $k \cdot p$ model [25] with the band-gap size determined by the calculated energy position of $S3$, 23 meV, reproduces well the linear dispersion of the R band as shown in Fig. 2(b), yielding an extremely light effective mass of $0.0074 \pm 0.0015 m_e$, where m_e is the electron rest mass. In fact, the $k \cdot p$ fitting is simple enough to treat the band-gap size as another free parameter, and the band gap is reliably determined to be within 18–24 meV [18] in good accord to the theoretical value. The effective mass determined is 20 times lighter than the normal Si LH band ($0.15 m_e$) [9]. Note also that, for the HH bands, the interband interaction is forbidden from the band symmetry [8]. Therefore, we conclude that the R band with an extremely linear dispersion is the modified LH band through the interband interaction with $S3$, while we do not know why the HH band itself is not observed around $\bar{\Gamma}_S$.

The $k \cdot p$ method has been widely applied to various semiconductors and the smallest effective mass reported is $0.016 m_e$ for InSb [9,18]. This yields the carrier mobility as high as 30 000 $\mathrm{cm^2\,V^{-1}\,s^{-1}}$, about 2 orders of magnitude higher than bulk Si [1]. The present effective mass for the Si IL, thus, indicates the possibility of an ultrafast carrier at Si interfaces. This method has not been applied to graphene and Bi compounds, for which only the effective mass values measured by transport experiments are available, about $(0.002–0.009) m_e$ in a similar range with the present value [2,5,18]. In contrast, the DFT calculation shown above does not reproduce exactly the linear dispersion of the LH band, yielding an effective mass of roughly $0.07 m_e$. We think this discrepancy is due to the limitation of the present slab calculation with only few Si layers in reproducing properly the QWS of the much thicker IL.

The proposed mechanism for the linear dispersion is summarized in Fig. 4(a). The contact of a metal film to a semiconductor substrate plays two key roles: (i) to induce a strong IL near the interface lifting the hole bands of the substrate up close to E_F and (ii) to provide a proper band

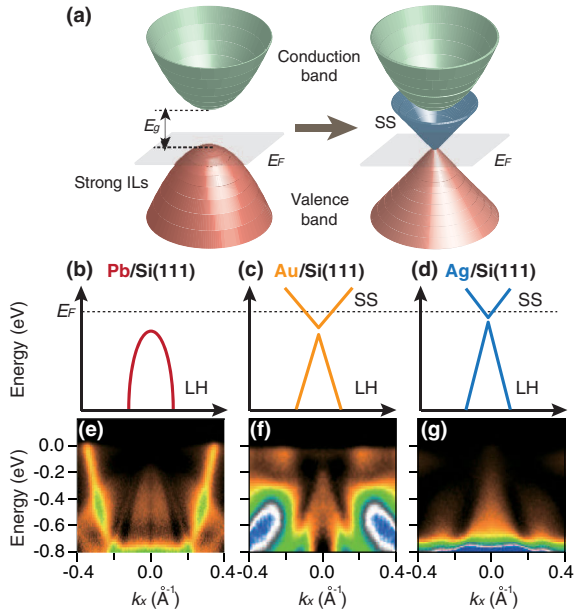

FIG. 4 (color online). (a) Schematic illustration of the mechanism for a linear hole band dispersion in semiconductor ILs. (b)–(d) Schematics of surface (SS) and LH band dispersions near $\bar{\Gamma}$ in Pb, Au, and Ag single-layer films on Si(111) with a common $\sqrt{3} \times \sqrt{3}$ symmetry [15,24,26]. (e)–(g) Corresponding ARPES dispersions of LH bands measured along the long arrow in Fig. 1(b) across $\bar{\Gamma}$.

($S3$ here) within the band gap inducing the strong repulsive interaction with hole bands for linear dispersion. In order to verify this mechanism, we took advantage of diverse surface band structures in metal-Si(111) systems. We examined three representative metal overlayers—Pb, Au, and Ag on Si(111)—with a common $\sqrt{3} \times \sqrt{3}$ symmetry but with different surface bands. Figs. 4(b)–4(d) describe corresponding band dispersions around $\bar{\Gamma}$ taken from previous reports in literature [15,24,26]. The $\sqrt{3} \times \sqrt{3}$-Pb system (with the Pb density of 4/3 ML) has no bands close to Si LH bands [15] while the others (at 1 ML) have adequate bands from the films similar to the present case to allow the interaction with the LH band (band gaps of 40–60 meV) [26,27]. The consequence of such a difference on the dispersion of the LH band is remarkable. In Fig. 4(e), our ARPES data for the Pb system show a normal parabolic dispersion consistent with bulk Si [8]. However, for Au and Ag systems, dispersions are obviously much more linear [Figs. 4(f) and 4(g)]. These results not only provide solid evidence on the validity of the proposed mechanism but also suggest the possibility of applications for a wider range of materials.

Our result suggests an unprecedented way to ultrafast electronic devices based on Si. Since this technique directly controls the carrier mass at the interface by a metal overlayer, it does not require any artificial modification or chemical engineering on the Si bulk lattice itself. Furthermore, this mechanism, in principle, can be generally applied to various other semiconductors even with thicker films [11], provided that proper interface states exist. For example, this may solve the notorious imbalance between the hole and electron mobility of III-V compounds [1].

This work was supported by KRF through the CRi program. M. H. K. acknowledges the support from KRF (Grant No. 2009-0074825).

*yeom@postech.ac.kr

[1] R. F. Service, Science **323**, 1000 (2009).
[2] K. S. Novoselov *et al.*, Nature (London) **438**, 197 (2005); Y. Zhang *et al.*, *ibid.* **438**, 201 (2005).
[3] T. Ohta *et al.*, Phys. Rev. Lett. **98**, 206802 (2007).
[4] L. Li *et al.*, Science **321**, 547 (2008).
[5] D. Hsieh *et al.*, Nature (London) **452**, 970 (2008).
[6] Y. Xia *et al.*, Nature Phys. **5**, 398 (2009).
[7] Y. L. Chen *et al.*, Science **325**, 178 (2009).
[8] J. H. Davies, *The Physics of Low-Dimensional Semiconductors* (Cambridge University Press, New York, 1998).
[9] P. Y. Yu and M. Cardona, *Fundamentals of Semiconductors* (Springer, Berlin, 2005).
[10] N. J. Speer, S.-J. Tang, T. Miller, and T. C. Chiang, Science **314**, 804 (2006).
[11] M. H. Upton, T. Miller, and T. C. Chiang, Phys. Rev. B **71**, 033403 (2005).
[12] P. Moras *et al.*, Phys. Rev. B **80**, 205418 (2009).
[13] S. Brochard *et al.*, Phys. Rev. B **66**, 205403 (2002).
[14] P. Cudazzo, G. Profeta, and A. Continenza, Surf. Sci. **602**, 747 (2007).
[15] W. H. Choi, H. Koh, E. Rotenberg, and H. W. Yeom, Phys. Rev. B **75**, 075329 (2007).
[16] T. Zhang *et al.*, Nature Phys. **6**, 104 (2010).
[17] S. Qin, J. Kim, Q. Niu, and C. -K. Shih, Science **324**, 1314 (2009).
[18] See supplementary material at http://link.aps.org/supplemental/10.1103/PhysRevLett.104.246803 for the sample characterization and the quantification of the effective mass.
[19] R. I. G. Uhrberg *et al.*, Phys. Rev. Lett. **52**, 2265 (1984).
[20] W. Mönch, *Semiconductor Surfaces and Interfaces* (Springer, Berlin, 2001).
[21] S. N. Takeda, N. Higashi, and H. Daimon, Phys. Rev. Lett. **94**, 037401 (2005).
[22] G. Kresse and J. Furthmüller, Phys. Rev. B **54**, 11 169 (1996).
[23] C. -H. Hsu, F. -C. Chuang, M. A. Albao, and V. Yeh, Phys. Rev. B **81**, 033407 (2010).
[24] C. Liu, I. Matsuda, R. Hobara, and S. Hasegawa, Phys. Rev. Lett. **96**, 036803 (2006).
[25] The dispersions of upper and lower bands are given by $E(k) = E_0 \mp E_g/2 + \frac{\hbar^2 k^2}{2m_e} \pm \sqrt{(E_g/2)^2 + (P \cdot k)^2}$.
[26] K. N. Altmann *et al.*, Phys. Rev. B **64**, 035406 (2001).
[27] H. J. Jeong, H. W. Yeom, and S. M. Jeong, Phys. Rev. B **77**, 235425 (2008).